View metadata, citation and similar papers at core.ac.uk
brought to you by CORE
provided by UCL Discovery

Identifiability, reducibility, and adaptability in allosteric macromolecules

Gergő Bohner[1]* and Gaurav Venkataraman[1,2]*

[1]Gatsby Computational Neuroscience Unit and [2]Wolfson Institute for Biomedical Research, University College London, London WC1E 6BT, England, UK

The ability of macromolecules to transduce stimulus information at one site into conformational changes at a distant site, termed "allostery," is vital for cellular signaling. Here, we propose a link between the sensitivity of allosteric macromolecules to their underlying biophysical parameters, the interrelationships between these parameters, and macromolecular adaptability. We demonstrate that the parameters of a canonical model of the *mSlo* large-conductance Ca^{2+}-activated K^+ (BK) ion channel are non-identifiable with respect to the equilibrium open probability-voltage relationship, a common functional assay. We construct a reduced model with emergent parameters that are identifiable and expressed as combinations of the original mechanistic parameters. These emergent parameters indicate which coordinated changes in mechanistic parameters can leave assay output unchanged. We predict that these coordinated changes are used by allosteric macromolecules to adapt, and we demonstrate how this prediction can be tested experimentally. We show that these predicted parameter compensations are used in the first reported allosteric phenomena: the Bohr effect, by which hemoglobin adapts to varying pH.

The Journal of General Physiology

INTRODUCTION

Cellular signaling relies on macromolecules to transduce stimuli information into conformational changes (Changeux and Edelstein, 2005). The mechanisms by which macromolecules accomplish this feat are often allosteric: a small stimulus applied at one area of the macromolecule regulates behavior at locations structurally distant from the active site of stimulation. A detailed and mechanistic understanding of allosteric regulation is a major goal of biophysics (Changeux, 2012, 2013). The Monod-Wyman-Changeux (MWC) model, which provides a physical-chemical interpretation of indirect regulation in terms of the geometry of the regulatory molecule (Monod et al., 1963, 1965; Marzen et al., 2013), has emerged as an essential tool in this effort. Operationally, any given MWC model represents a candidate hypothesis for how allosteric conformational change occurs. If a model is not able to quantitatively fit available data, it is rejected. For models that agree with the data, the model parameter values provide estimates of biophysically meaningful properties that cannot be measured directly. Tremendous effort has gone toward determining which mechanistically relevant parameters best fit available macromolecular data (Colquhoun and Hawkes, 1982, 1995; Horn and Lange, 1983; Blatz and Magleby, 1986; Ball and Sansom, 1989; Kienker, 1989; Ball and Rice, 1992; Colquhoun and Sigworth, 1995; Qin et al., 1996, 2000; Colquhoun et al., 2003; Celentano and Hawkes, 2004; Milescu et al., 2005; Moffatt, 2007). However, it has recently been observed that even simple MWC models suffer from parameter non-identifiability: the data in commonly used activity (or binding) curves do not provide sufficient constraining power to find unique values of the parameters, even if essentially noiseless (Hines et al., 2014; Middendorf and Aldrich, 2017a,b).

Essentially all work on parameter estimation in MWC models has treated non-identifiability as a hurdle to be overcome toward the estimation of individual MWC parameter values, which clearly confer mechanistically meaningful information about the macromolecule under study. Here, we argue that valuable mechanistic information may be lost by focusing on individual parameter values. We demonstrate that non-identifiable datasets admit identifiable "emergent" parameters and argue that these emergent parameters confer mechanistic information about macromolecular function not available from individual parameter values themselves, no matter how accurate.

We begin by studying the causes of parameter non-identifiability in a canonical MWC model of the *mSlo* large-conductance Ca^{2+}-activated K^+ (BK) ion channel (Horrigan and Aldrich, 2002; Yan and Aldrich, 2010), with respect to two common assays of functional activity. The non-identifiability is shown

*G. Bohner and G. Venkataraman contributed equally to this paper.
Correspondence to Gaurav Venkataraman: gaurav@alumni.reed.edu
G. Venkataraman's present address is Division of Medicine, University College London, London WC1E 6BT, England, UK.

Abbreviations used: BK, *mSlo* large-conductance Ca^{2+}-activated K^+; MBAM, manifold boundary approximation method; MWC, Monod-Wyman-Changeux.

© 2017 Bohner and Venkataraman This article is distributed under the terms of an Attribution–Noncommercial–Share Alike–No Mirror Sites license for the first six months after the publication date (see http://www.rupress.org/terms/). After six months it is available under a Creative Commons License (Attribution–Noncommercial–Share Alike 4.0 International license, as described at https://creativecommons.org/licenses/by-nc-sa/4.0/).

The Rockefeller University Press $30.00
J. Gen. Physiol. 2017 Vol. 149 No. 5 547–560
https://doi.org/10.1085/jgp.201611751

Check for updates

to arise because the parameters compensate for each other to produce similar model output, rather than because the model contains irrelevant parameters. In particular, we demonstrate that observed parameter non-identifiability is caused by "sloppy" sensitivity of parameters to model output: the model output is highly sensitive to particular nonlinear combinations of parameters and essentially insensitive to others (Brown and Sethna, 2003; Waterfall et al., 2006; Gutenkunst et al., 2007; Transtrum et al., 2010, 2011, 2015).

We address the issue of parameter non-identifiability by constructing "reduced" models of the channel for each of the two functional assays, using the recently developed manifold boundary approximation method (MBAM; Transtrum and Qiu, 2014; Transtrum, 2016 *Preprint*). Each reduced model has fewer parameters than the original model but describe its functional data equally well. Crucially, the parameters of these reduced models are (a) identifiable with respect to the model output and (b) explicitly expressed as emergent combinations of the original MWC parameters. Our reduced models therefore allow for quantitative estimates of biophysically relevant parameters, despite individual parameter non-identifiability.

The emergent parameters of our reduced models indicate which coordinated changes in biophysical parameters may preserve assay output. We therefore interpret our reduced models as predictions encoded in the original MWC model. These predictions confer information about the robustness of a macromolecule's underlying biophysical parameters with respect to a functional output. We claim that these predictions have physiological and evolutionary relevance, so long as the model is mechanistically relevant and the functional assay adequately captures the macromolecule's in vivo function.

It is difficult to determine confidently that any given assay or set of assays captures a macromolecule's in vivo behavior. Here, we choose to study equilibrium binding curves, thereby adopting the hypothesis that the in vivo purpose of a macromolecule is to act as a biological sensor that takes stimuli information as input and produces equilibrium activity as output; this hypothesis is common in information-theoretical studies of MWC models (Tkacik et al., 2008; Martins and Swain, 2011; Olsman and Goentoro, 2016).

Ultimately, the relevance of our predicted parameter compensations, and thereby our assay choice, must be determined experimentally. To this end, we demonstrate that a previous meta-analysis of hemoglobin oxygen-binding curves confirms the physiological relevance of parameter compensations in hemoglobin's adaptation to varying pH, referred to as the Bohr effect and known to be important for the efficient transportation of oxygen through blood in vivo.

MATERIALS AND METHODS

The full code used to generate the synthetic data and all analyses is available on GitHub: https://github.com/gbohner/MBAM.

Synthetic data generation

Our model takes as input N voltage and calcium pairs as an array $\mathbf{X}$, and an $M \times 1$ vector of parameters $\boldsymbol{\theta}$. The output of the model is an $N \times 1$ vector of open probabilities $\mathbf{y}$. We represent the model as the function $f(\boldsymbol{\theta},\mathbf{X}) = \mathbf{y}$, defined as in the text. Our "base" parameters $\boldsymbol{\theta}^*$ (Fig. 2 B) were chosen to match previous studies (Horrigan and Aldrich, 2002; Miranda et al., 2013).

Fitting noisy data

Given a $\boldsymbol{\theta}$ to be estimated, noisy data $\mathbf{y'}$ were generated from mode $f(\boldsymbol{\theta},\mathbf{X})$ via

$$\mathbf{y'} = f(\boldsymbol{\theta},\mathbf{X}) \odot \epsilon(\sigma),$$

where $\varepsilon(\sigma)$ is drawn from the distribution Uniform($[1 - \sigma, 1 + \sigma]$). Additive and multiplicative Gaussian noise models were also tested.

We then used the Levenberg-Marquardt solver (Marquardt, 1963) to infer the best-fit parameters $\boldsymbol{\theta'} = \mathrm{argmin}_{\boldsymbol{\theta}} \mathscr{C}(\boldsymbol{\theta},\mathbf{y'})$, where $\mathscr{C}(\boldsymbol{\theta},\mathbf{y'}) = \mathscr{C}\|f(\boldsymbol{\theta},\mathbf{X}) - \mathbf{y'}\|$ is the norm of the discrepancy between data and model output. Each fit was performed from 24 different initial parameter vectors, from which the global best-fit parameters were selected.

Computing relative parameter error

Σ_i, a lower bound on the relative size of the 95% confidence interval for the i-th parameter, was calculated (Gutenkunst et al., 2007; Apgar et al., 2010):

$$\Sigma_i = \exp\left(4 \times \left(\frac{\sigma^2}{N}\left(\mathbf{H}_{\boldsymbol{\theta}}^{-1}\right)_{i,i}\right)^{1/2}\right) - 1,$$

where

$$\mathbf{H}_{\boldsymbol{\theta}} = \frac{d^2}{d\log\boldsymbol{\theta}^2}\mathscr{C}(\boldsymbol{\theta},\mathbf{y}).$$

The log Hessian $\mathbf{H}_{\boldsymbol{\theta}}$ is used to estimate the widths of the constant cost ellipsoid (Fig. 3 B), and the diagonal elements of its inverse are used to place a lower bound on individual relative parameter errors, Σ_i. For all of our calculations, $N = 104$ and $\sigma = 10\%$.

MBAM

MBAM attempts to reduce the number of parameters in a model while quantitatively fitting a given dataset. This is accomplished by reducing the number of parameters in a model one at a time. Each single parameter reduction is the result of eliminating or combining diverging

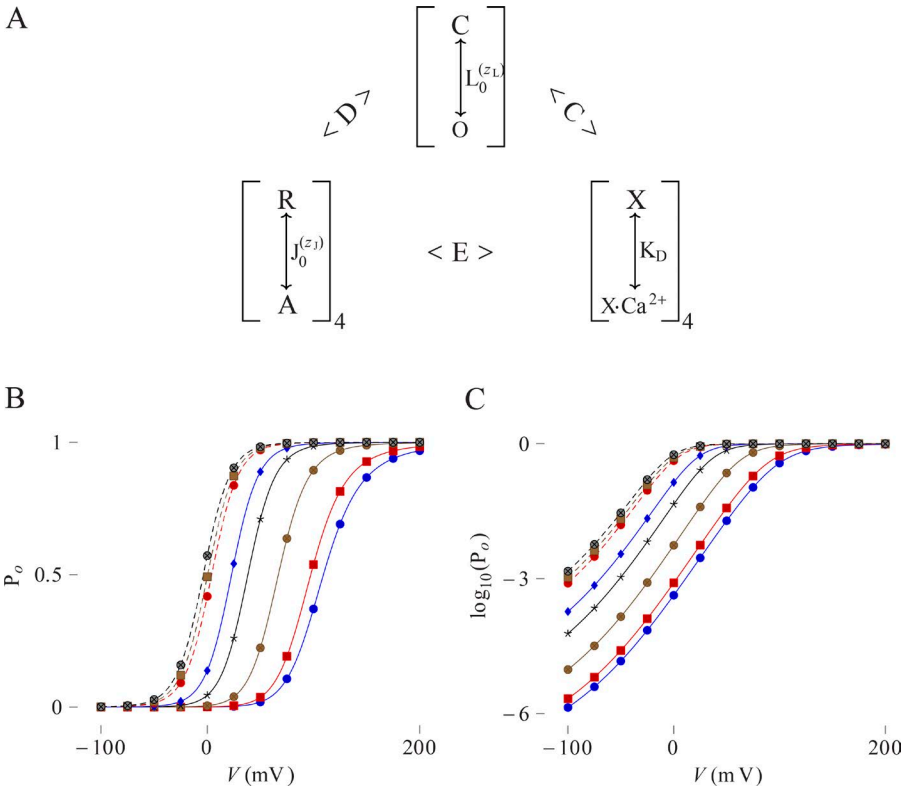

Figure 1. **Synthetic steady-state data.** (A) Schematic of the general allosteric gating mechanism used to generate synthetic data. Subscripts denote the number of identical subunits. The steady-state properties of this model are fully described by eight parameters $\{L_0, z_L, J_0, z_J, K_D, C, D, E\}$. (B and C) $P_o - V$ and $\log(P_o) - V$ relationships generated from base parameters (Fig. 2 B) for different Ca^{2+} concentrations (μM: 0 [blue circles]; 0.7 [red boxes]; 4 [brown crossed circles]; 12 [asterisks]; 22 [blue diamonds]; 55 [red circles]; 70 [brown boxes; 95 [gray crossed circles]). For each Ca^{2+}, voltage was sampled uniformly in 25-mV intervals.

parameters. These diverging parameters are found by searching through parameter space along a trajectory that minimizes the effect on model output. Such a trajectory is found by solving the following system of ordinary differential equations,

$$\frac{d}{dt}\boldsymbol{\theta}_t = \mathbf{v}_t$$
$$\frac{d^2}{dt^2}\boldsymbol{\theta}_t = -\left[(\nabla \mathbf{r}_t)(\nabla \mathbf{r}_t)^{\top}\right]^{-1}(\nabla \mathbf{r}_t)\frac{\mathbf{v}_t^{\top}\mathbf{H}_{\boldsymbol{\theta}_t}\mathbf{v}_t}{\|\mathbf{v}_t\|^2},$$

where t denotes time spent following the trajectory, $\mathbf{H}_{\boldsymbol{\theta}_t}$ refers to the log Hessian evaluated at $\boldsymbol{\theta}_t$ as defined above, $\mathbf{r_t} = f(\boldsymbol{\theta}_t, \mathbf{X}) - f(\boldsymbol{\theta}^*, \mathbf{X})$ is the vector of output discrepancies for all inputs, and ∇ denotes the vector gradient operation with respect to the parameters.

The initial parameter vector $\boldsymbol{\theta}_0$ is taken to be the vector of presumed best-fit parameters $\boldsymbol{\theta}_0 = \boldsymbol{\theta}^*$, and the initial direction vector ($\mathbf{v}_0$) is set to be the sloppiest direction of the constant cost ellipsoid. These initial conditions enforce that our search begins at the lowest point of our cost surface ($\boldsymbol{\theta}_0$) and that we initially move in the direction that goes uphill as little as possible ($\mathbf{v}_0$). This trajectory is followed until the diverging parameters are found ($\boldsymbol{\theta}_{t_{\text{end}}}$), or the cost becomes so large that the parameters no longer fit the data. The reader is referred to Transtrum (2016) (*Preprint*) and Transtrum and Qiu (2014, 2016) for full details.

Online supplemental material

Our supplemental text contains full algebraic details of the MBAM reductions presented in the paper. Fig. S1 shows RMS cost for each reduced model. Fig. S2 shows how parameter compensations explain the discrepancy between true and inferred values. Fig. S3 shows inferred parameters from the reduced $\log(P_o)$ model.

RESULTS

The BK channel primarily senses two stimulus signals: membrane voltage and intracellular Ca^{2+} concentration (Horrigan and Aldrich, 2002; Latorre and Brauchi, 2006; Yan and Aldrich, 2010; Miranda et al., 2013). In response to these signals, BK opens its channel gate, allowing potassium ions to permeate. We consider a canonical model of BK gating (Horrigan and Aldrich, 2002; Yan and Aldrich, 2010), shown schematically in Fig. 1 A. The model consists of three functional domains: the channel gate, voltage-sensing domain, and Ca^{2+}-sensing domain. The channel gate is regulated by four identical and independent voltage and Ca^{2+} sensors. Consistent with the MWC framework, each domain can be in one of two conformations: C-O, R-A, X - X · Ca^{2+} for the gate, voltage, and Ca^{2+} subunits, respectively. The function of each domain is defined by an equilibrium constant (L, J, K), and the coupling between domains is mediated by allosteric factors (C, D, E). Formally, the model is given by

$$P_o(V, [\mathrm{Ca}^{2+}]) = \frac{L(1 + KC + JD + JKCDE)^4}{L(1 + KC + JD + JKCDE)^4 + (1 + J + K + JKE)^4}, \quad (1)$$

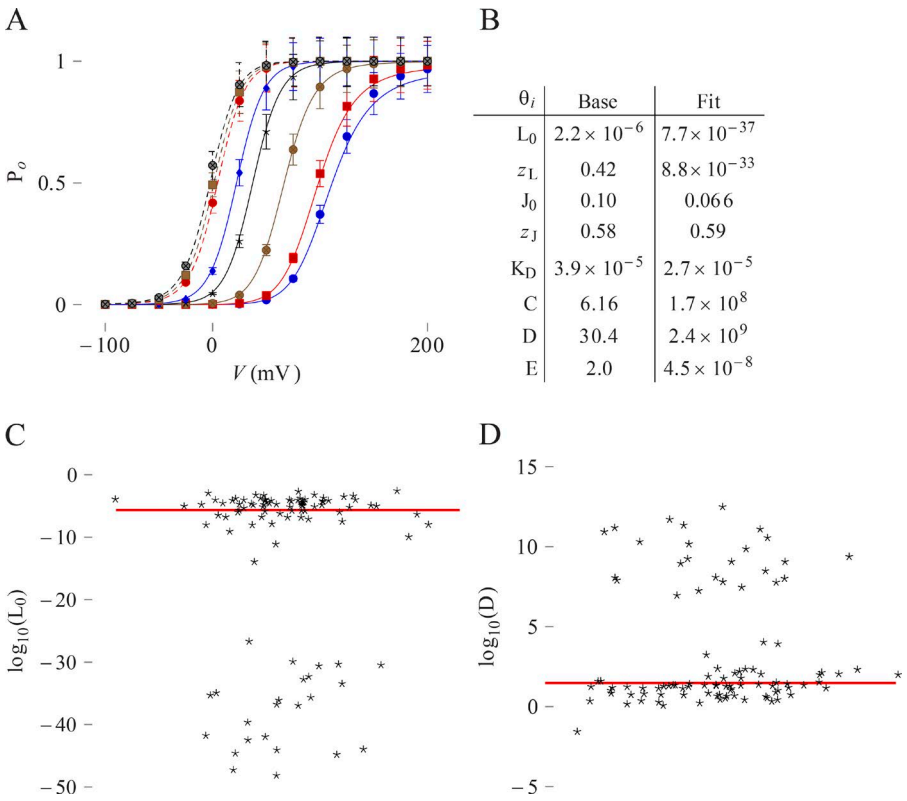

θ_i	Base	Fit
L_0	2.2×10^{-6}	7.7×10^{-37}
z_L	0.42	8.8×10^{-33}
J_0	0.10	0.066
z_J	0.58	0.59
K_D	3.9×10^{-5}	2.7×10^{-5}
C	6.16	1.7×10^{8}
D	30.4	2.4×10^{9}
E	2.0	4.5×10^{-8}

Figure 2. **An illustration of non-identifiability.** (A) Data generated with base parameters, well fit with fit parameters. Error bars are 10% from noiseless data value. Data are labeled as in Fig. 1. (B) Parameters that generated the data (base) and the solid lines (fit) shown in A. z_L and z_J are in units of e, K_D is in units of M; the other parameters are dimensionless. (C and D) Log of fitted L_0, D (respectively) values to 100 noisy synthetic P_o datasets generated from base parameter values. Values span many orders of magnitude. The horizontal spread is for ease of visualization; red lines indicate the true base parameter.

with equilibrium constants (J, K, L) given by

$$L = L_0\exp\left(\frac{-z_L V}{kT}\right);\ J = J_0\exp\left(\frac{-z_J V}{kT}\right);\ K = \frac{[Ca^{2+}]}{K_D},$$

where z_L and z_J are the partial charges associated with channel opening and voltage sensor activation, respectively. Synthetic data generated from this model is shown in Fig. 1 (B and C).

The biophysical parameters {L_0, z_L, J_0, z_J, K_D, C, D, E} in Eq. 1 have been estimated with a wide variety of experimental assays. We will focus on the identifiability of these parameters with respect to the steady-state open probabilities of BK at various voltages and Ca^{2+} concentrations. In the language of MWC models, this "P_o" curve corresponds to the ubiquitous activity or binding curve. We will also analyze a related common assay (Horrigan and Aldrich, 2002): the base 10 logarithms of the probabilities, $\log(P_o)$, made possible by single-channel recordings that allow for the determination of very small steady-state open probabilities. We will see that the model exhibits non-identifiability with respect to both assays, but the non-identifiability is more severe for the P_o assay. We will demonstrate that this difference in non-identifiability implies that the $\log(P_o)$ assay may be used to experimentally test for the presence of parameter compensations predicted to hold the P_o assay constant.

BK parameters are non-identifiable because of sloppiness

We begin by asking the following: how identifiable are the BK model parameters, with respect to each of the P_o and $\log(P_o)$ assays? Fig. 2 illustrates the problem of non-identifiability via the P_o assay: noisy synthetic data generated from the BK model are well fit (within the 10% error bars) by parameter values far from the base values used to generate the data (Fig. 2, A and B). To get a sense of how widely the parameters inferred from noisy P_o data may vary, we fit the P_o model to 100 noisy synthetic P_o datasets (see Materials and methods) generated from the base parameters. We found that the best-fit parameters to noisy data spanned many orders of magnitude; the inferred best-fit parameters for L_o, D are shown in Fig. 2 (C and D). We investigated BK model identifiability systematically by computing lower bounds on the relative parameter error (see Materials and methods) around the base parameter values. Many parameters have significant errors with respect to each assay (Fig. 3 A). The model suffers from non-identifiability.

It has been argued that non-identifiability in scientific models arises because of sloppiness: the model output is extremely sensitive to some combinations of parameters but dramatically insensitive to other combinations (Gutenkunst et al., 2007; Machta et al., 2013). We there-

A

Parameter (θ_i)	L_0	z_L	J_0	z_J	K_D	C	D	E
P_o Relative error (%)	5×10^{11}	4.0×10^{4}	7.4×10^{3}	71.80	304.31	2.8×10^{3}	1.8×10^{6}	1.7×10^{4}
$\log(P_o)$ Relative error (%)	7.9×10^{3}	612.18	262.10	9.50	13.14	32.88	1.2×10^{3}	22.19

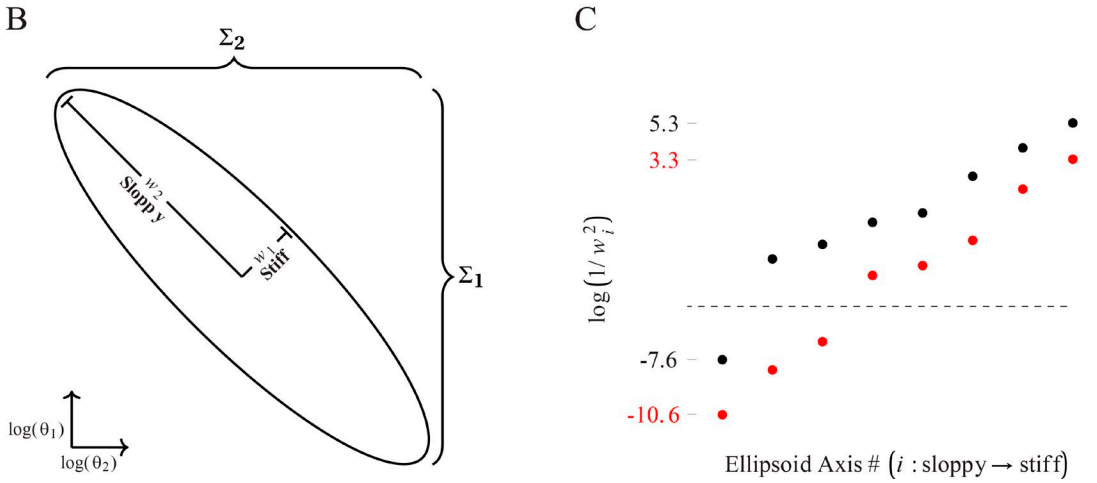

Figure 3. **The BK model is sloppy.** (A) Lower bounds on parameter error (95% confidence interval) for each of the P_o, $\log(P_o)$ assays. The P_o assay exhibits much worse identifiability than the $\log(P_o)$ assay. (B) Ellipsoid of constant cost for a toy two-parameter model. The center point of the ellipsoid are the best-fit parameters. The parameters $\theta_{1,2}$ are constrained in the stiff direction, but have large error regions $\Sigma_{1,2}$ because of the presence of a large sloppy direction. w_i denotes the length of axis i. (C) Calculated $\log(1/w_i^2)$ values for the P_o assay (red) and $\log(P_o)$ assay (black). Both exhibit a linear trend, the signature of a sloppy model. The dashed line is a visual aid aimed to draw attention to the gap in the data points.

fore ask: do either of the P_o, $\log(P_o)$ assays exhibit sloppiness with respect to the underlying BK model parameters?

Formally, sloppiness is a feature of a model's approximate "surface of constant cost." To understand sloppiness, it is therefore useful to consider a surface of constant cost for a toy two-parameter model (Fig. 3 B). The toy surface is an ellipse that sits in parameter space, centered around the presumed best-fit parameters. In general, the surface of constant cost will have dimension equal to the number of model parameters. Each point on a surface of constant cost identifies parameters whose model output is equivalently different from the output generated by the best-fit parameters, as measured by a cost function. Most commonly, this cost function is the root-mean-squared (RMS) error.

The toy constant cost ellipse illustrates the two key features of sloppiness. (1) One axis of the ellipse is much longer than the other ($w_2 >> w_1$); one direction of parameter space therefore constrains model behavior much more than the other. (2) The ellipse is "tilted" rather than aligned with the parameter axes, so each ellipse axis corresponds to a combination of the two parameters. The toy ellipse therefore asserts that some combinations of parameters constrain the model behavior much more than others. The degree to which a parameter combination constrains the model output is encoded in the length of its axis (w_i). The error bars for the toy parameters θ_1, θ_2 are given by Σ_1, Σ_2. Although the model is constrained by the combination of the two parameters in the "stiff" direction of parameter space, neither individual parameter is well constrained.

Because the BK model has many more than two parameters, we cannot easily visualize its ellipsoid of constant cost. We therefore assessed BK model sloppiness by computing a quantity proportional to the lengths of the axes of its constant cost ellipsoids, $1/w_i^2$ (Fig. 3 C). Each assay exhibits the striking signature of sloppy models: the $1/w_i^2$ are exponentially spaced, corresponding to a linear spacing in logarithm (Waterfall et al., 2006). The P_o assay (Fig. 3 C, red marks) exhibits a greater degree of sloppiness than the $\log(P_o)$ assay (Fig. 3 C, black marks), consistent with the $\log(P_o)$ assay having more identifiable parameters than the P_o assay (Fig. 3 A). Note that each data point in Fig. 3 C corresponds to an axis of the ellipsoid of constant cost, and in general, each axis will correspond to a combination of parameters, as shown in Fig. 3 B. There exists a visible gap (Fig. 3 C, dashed line) between the more sloppy (below line) and more stiff (above line) widths for both assays. Although such a clear gap does not likely exist in general, we will later observe that the minimal number of model reductions needed to produce an identifiable model is equal to the number of axes having widths below this dashed line. This foreshadowing is consistent

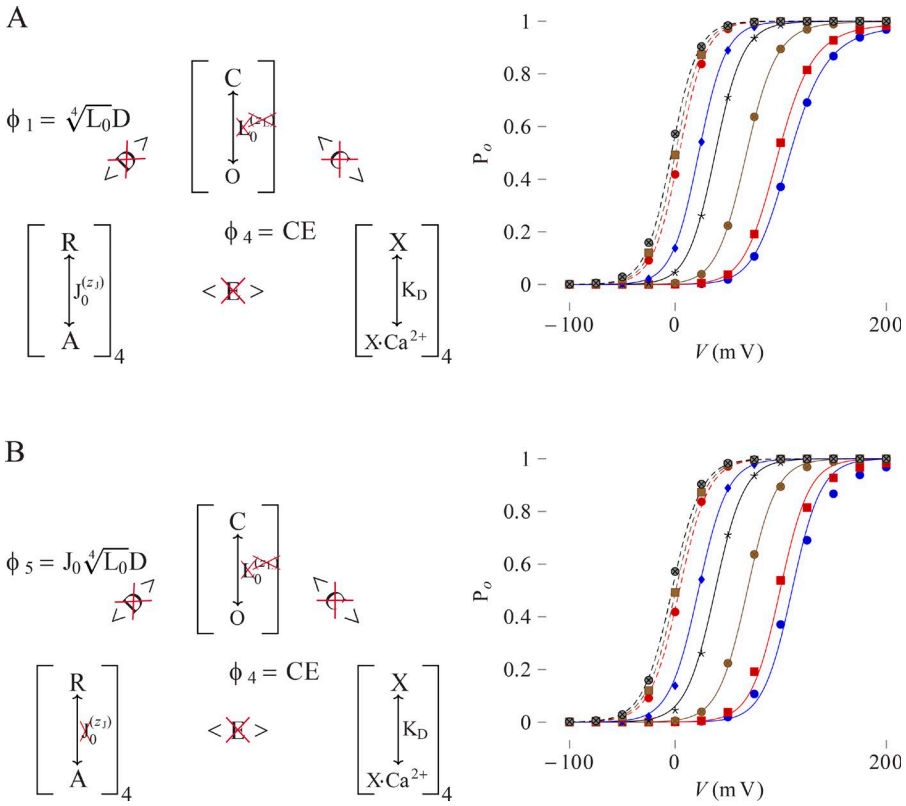

Figure 4. **Results of model reduction for the P_o assay.** (A, left) Schematic of the model admitted by the third reduction; five parameters have been eliminated from the original model (red crosses) and two new emergent parameters have been added ($\phi_{1,4}$) for a total reduction of three parameters. (A, right) This model fits the data (solid lines) extremely well. (B, left) Schematic of model admitted by the fourth reduction. (B, right) This model does not fit the data well at low [Ca^{2+}]. Synthetic data are labeled as in Fig. 1 (B and C).

with the fact that the model reduction procedure leverages the geometry of the model parameter space to remove existing sloppiness.

A reduced model for the P_o assay admits identifiable emergent parameters

Having shown that the BK model has non-identifiable parameters because of sloppiness, we now aim to exploit the model's sloppiness to construct new BK models whose parameters are both identifiable and of mechanistic interest. To construct such models, we use the MBAM (Transtrum and Qiu, 2014; Transtrum, 2016 *Preprint*).

The MBAM algorithm takes three items as input: data, a mathematical model thought to describe the data, and the parameters of the model thought to best fit the data. The goal of the algorithm is to find a point in parameter space having two properties: (1) the model output generated by the parameters must fit the data well; and (2) one or more parameters must be divergent, having values close to 0 or ∞. To find such a point, the algorithm searches through parameter space, along a trajectory that minimizes the effect on model output. The search terminates once divergent parameters are found, and the model is reparameterized such that no parameters equal to 0 or ∞ remain. The algorithm is made to repeat until the newly parameterized models no longer fit the data well (see Materials and methods). The algorithm is deterministic: run on the same data with the same initial conditions, it will return the same reductions.

An overview of our MBAM output with respect to the P_o assay is shown in Fig. 4. MBAM was run on a set of synthetic data points generated from the BK model and initialized with the "true" BK model parameters that generated these data points. The algorithm was terminated after five iterations, each of which reduced the number of model parameters by one. The first three MBAM iterations produced models that fit the data essentially exactly (Fig. S1). The model produced by the third reduction step (Fig. 4 A) has eliminated five parameters and introduced two new emergent parameters, $\phi_1 = \sqrt[4]{L_0}\,D$, $\phi_4 = CE$. The model produced by the fourth step (Fig. 4 B, left) does not fit the data well at low calcium concentrations (Fig. 4 B, right).

To better understand how the reduced models arise, we plotted the numerical values of the model parameters during MBAM searches (Fig. 5, left) and the resulting reduced models (Fig. 5, right). Because MBAM searches along a trajectory of essentially equivalent model behavior, each x-axis "time point" corresponds to a set of parameter values that produce essentially equivalent model output (Fig. 5, left). The algorithm continues searching until one or more parameters diverge to zero or infinity (Fig. 5, red lines). It is interesting to note that as z_L goes to zero (Fig. 5 A, red line), several nondivergent parameters must compensate (Fig. 5 A, curved black lines) to fit the synthetic data. Subsequent

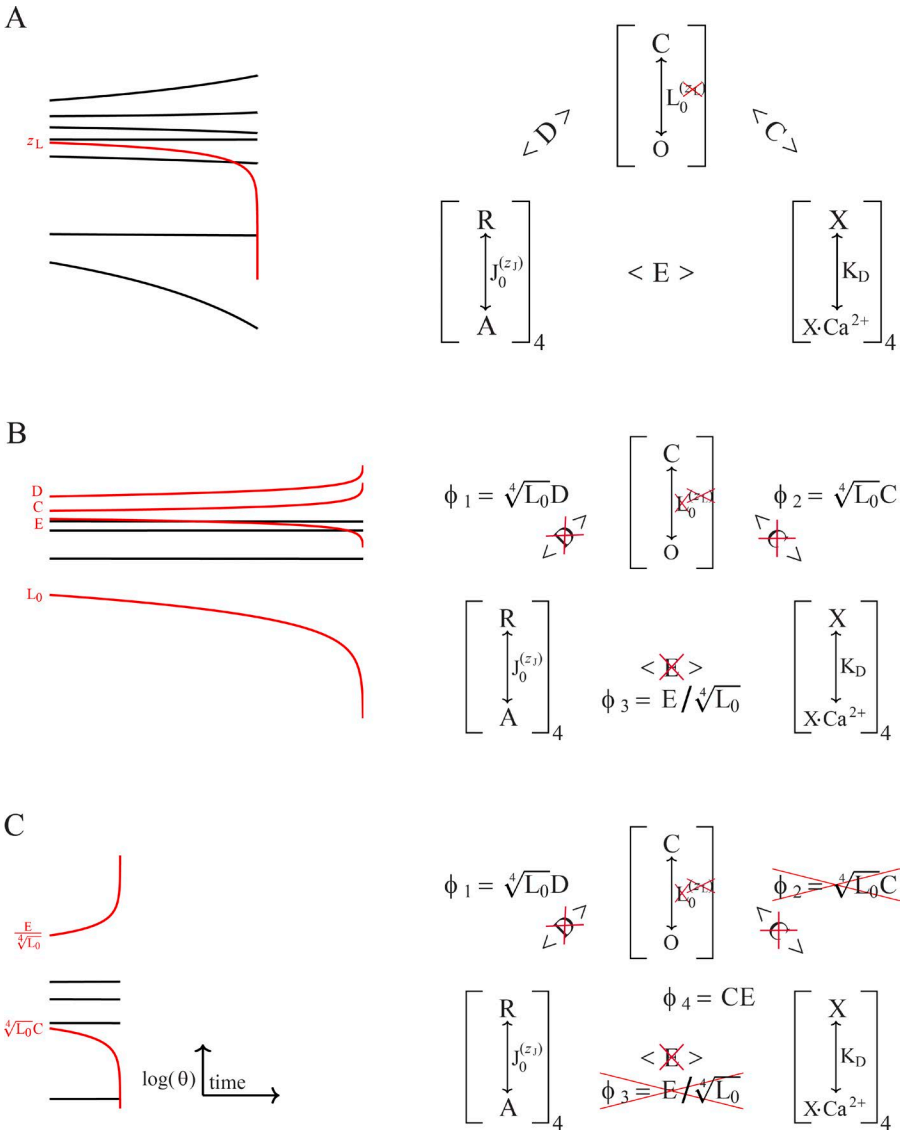

Figure 5. **Intermediate MBAM steps, P_o assay.** The figure should be read left to right, top to bottom. The left column displays the parameter values for a given model as MBAM progresses. The reduced model created upon completion of the parameter search is displayed on the right. (A) MBAM run for the full, original model. There are eight lines, corresponding to eight parameters. One of the parameters goes to zero; this is z_L, and it is eliminated, giving our first reduced model, at right. (B) In the second iteration, four parameters are observed to diverge: L_0, D, E, C. These parameters are eliminated, and three new, emergent parameters are created ($\phi_{1,2,3}$), yielding a net reduction of one parameter. (C) Two parameters are observed to diverge: ϕ_2, ϕ_3. Note that there are only six lines, corresponding to the six remaining parameters. The resulting model (right) has five parameters and fits the data well (Fig. 4).

reductions (Fig. 5, B and C) take place without such significant compensation from nondiverging parameters.

The algebraic reparameterizations that give rise to the reduced models in Fig. 5 are worked out in full in the Supplemental text. To understand the emergent parameters biologically, it is instructive to consider the third and "final" reduced model, which is algebraically governed by

$$P_o\left(V,[Ca^{2+}]\right) = \frac{(J\phi_1)^4(1+K\phi_4)^4}{(J\phi_1)^4(1+K\phi_4)^4+(1+J+K)^4}, \qquad (2)$$

with equilibrium constants (J, K) given by

$$J = J_0\exp\left(\frac{-z_J V}{kT}\right);\ K = \frac{[Ca^{2+}]}{K_D}.$$

The emergent parameter $\phi_4 = CE$ represents the effect of $[Ca^{2+}]$ binding on the voltage-sensing process, and $\phi_1 = \sqrt[4]{L_0}\,D$ represents the coupling of voltage sensing to the pore opening. Additionally, the remaining original parameter K_D is the binding constant of the ligand, J_0 governs the midpoint voltage of the voltage-activation curve, and z_J controls its slope.

We next ask: do the reduced models have identifiable parameters? To address this issue, we calculated lower bounds on the relative error for each of the reduced models and found that each reduction step leads to a model with fewer unidentifiable parameters (Fig. 6). It is important to note that although each model reduction step leads to a smaller number of non-identifiable parameters than the one before it, it is not the case that each parameter becomes more identifiable after each reduction step. In the first reduced model, L_0, C, D, and E and all have much greater relative errors than in the original model (compare Fig. 6 A [table] with Fig. 3 A). Care must therefore be taken in interpreting these intermediate models (Fig. 6, A and B).

In contrast, interpreting the third reduced model (Fig. 6 C) is clear. The model fits the data extremely

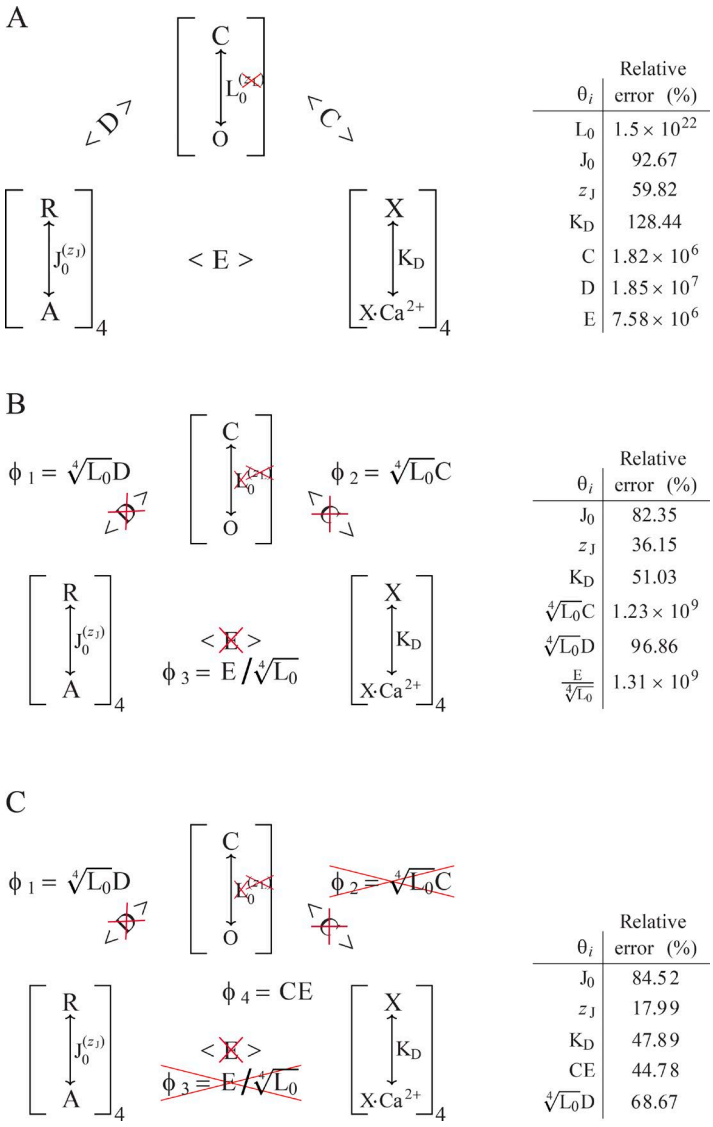

A

θ_i	Relative error (%)
L_0	1.5×10^{22}
J_0	92.67
z_J	59.82
K_D	128.44
C	1.82×10^{6}
D	1.85×10^{7}
E	7.58×10^{6}

B

θ_i	Relative error (%)
J_0	82.35
z_J	36.15
K_D	51.03
$\sqrt[4]{L_0}C$	1.23×10^{9}
$\sqrt[4]{L_0}D$	96.86
$\frac{E}{\sqrt[4]{L_0}}$	1.31×10^{9}

C

θ_i	Relative error (%)
J_0	84.52
z_J	17.99
K_D	47.89
CE	44.78
$\sqrt[4]{L_0}D$	68.67

Figure 6. **Model reduction results in identifiable parameters.** Reduced models for the P_o assay are presented in the left column, and error lower bounds of their parameters (95% confidence interval) are presented at right. A–C correspond to model-error pairs after one, two, and three reduction steps, respectively. The five-parameter model produced by three model reductions (C, left) has identifiable parameters (within one order of magnitude for all parameters, right).

well (Fig. 4 A) and has parameters that are identifiable and expressed in terms of mechanistically meaningful parameters (Fig. 6 C, table). Variations in underlying MWC parameters that keep these emergent parameters constant may, but do not necessarily, leave assay output unchanged. Conversely, any significant parameter variation that leaves the P_o assay unchanged must keep the emergent parameters constant. Observe that the differences in base and fit parameters that give rise to the same dataset in Fig. 2 B do indeed keep the emergent parameters essentially constant. Relative to the base parameter, the fit parameter C increased by a factor of 10^8; correspondingly, the parameter E decreased by a factor of 10^8, consistent with constant emergent parameter $\phi_4 = CE$. Likewise, the value of $\sqrt[4]{L_0}$ decreased by a factor of 10^8, and correspondingly the value of D increased by a factor of 10^8, consistent with constant emergent parameter $\phi_1 = \sqrt[4]{L_0}\,D$.

We interpret the emergent parameters as predictions of the original MWC model about potential compensatory mechanisms of the macromolecule. How can we test for the presence of these parameter compensations experimentally? By definition, the compensations are not discernible from the P_o assay. To address this issue, we therefore turn to the $\log(P_o)$ assay.

The $\log(P_o)$ model reduction reveals parameter differences unidentifiable by P_o

Having found a reduced, identifiable model for the P_o assay, we now aim to find such a model for the $\log(P_o)$ assay. Because the $\log(P_o)$ assay was observed to have fewer "very sloppy" directions than the P_o assay (Fig. 3 C), we expected to find an identifiable model after fewer reduction steps than needed for the P_o assay. Indeed, MBAM produces an identifiable model after only one reduction step. In this model, each of the orig-

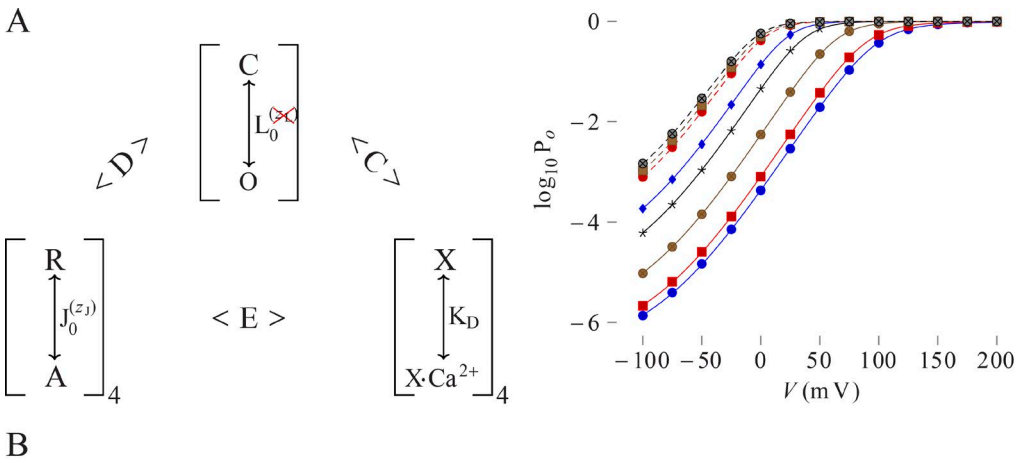

B

Parameter (θ_i)	L_0	J_0	z_J	K_D	C	D	E
Relative error (%)	68	43	5.6	11	16	52	23

Figure 7. **Reduced log(P_o) model.** (A) A model resulting from one reduction (left) fits synthetic data (right; data legend as in Fig. 1) very well (solid lines). (B) This model has identifiable parameters.

inal parameters is identifiable except for z_L, which has been eliminated (Fig. 7).

Can we use the reduced log(P_o) model to detect the presence of large compensatory parameter changes that give rise to identical P_o datasets? To address this issue, we generated test and base parameters that produced equivalent P_o data (up to 10% error), but contained the type of large compensatory changes shown in Fig. 2 B. The test and base parameters were then used to generate noisy synthetic log(P_o) data, to which the reduced log(P_o) model was fit. Values of the base parameters inferred by the reduced log(P_o) model varied many orders of magnitude less than when inferred from noisy P_o data generated from the same parameters (compare the black points in Fig. 8 [A and B] with Fig. 2 [C and D]), reflecting the greater identifiably of the reduced log(P_o) model.

This increase in identifiability allows the reduced log(P_o) model to discern large compensatory parameter changes that leave the P_o assay constant (Fig. 8, red points). Note that the mean of the inferred parameter values (Fig. 8, solid lines) did not match the true values of the underlying parameters (Fig. 8, dashed lines). This is expected because of compensations from the other parameters (Fig. S2) and does not affect discernibility. Our analysis is limited in that we did not exhaustively sample the parameter space. Rather, we examined several sets of test parameters and found that large compensatory variations from the base parameters were discerned via the reduced log(P_o) model in all cases, even when the test parameters were degenerate (Fig. S3). We wish here only to make the point that the log(P_o) assay can elucidate parameter variations hidden by the P_o assay in practice, not that it must in general.

DISCUSSION

Our results demonstrate that reduced models produced by MBAM allow for quantitatively accurate parameter information to be gleaned from models that are non-identifiable with respect to most or all individual parameters. Because the emergent parameters of our reduced models indicate which coordinated changes in parameter values are necessary to preserve the output for a given assay, they may be interpreted as predictions of the MWC model about which biophysical properties can compensate for each other to maintain a functional role. For what purposes would MBAM-elucidated compensatory effects be used by allosteric macromolecules? We propose experiments to test the role of parameter compensation in functional and evolutionary adaptation, both of which have been previously connected to sloppiness (Daniels et al., 2008).

Emergent parameters may facilitate functional adaptation

It is well known that macromolecules exhibit some amount of functional robustness with respect to experimental perturbations of temperature, pH, salt conditions, and sequence structure (Rennell et al., 1991; Somero, 1995; Suckow et al., 1996; Guo et al., 2004; Weber and Pande, 2012). We propose that this functional robustness may arise from compensatory mechanisms of the type identified here. That is, changes in environment or sequence structure that have little effect on assay output should be observed to have large but compensatory effects in the mechanistic parameters, such that the value of MBAM-identified emergent parameters remain constant. In BK, for example, we

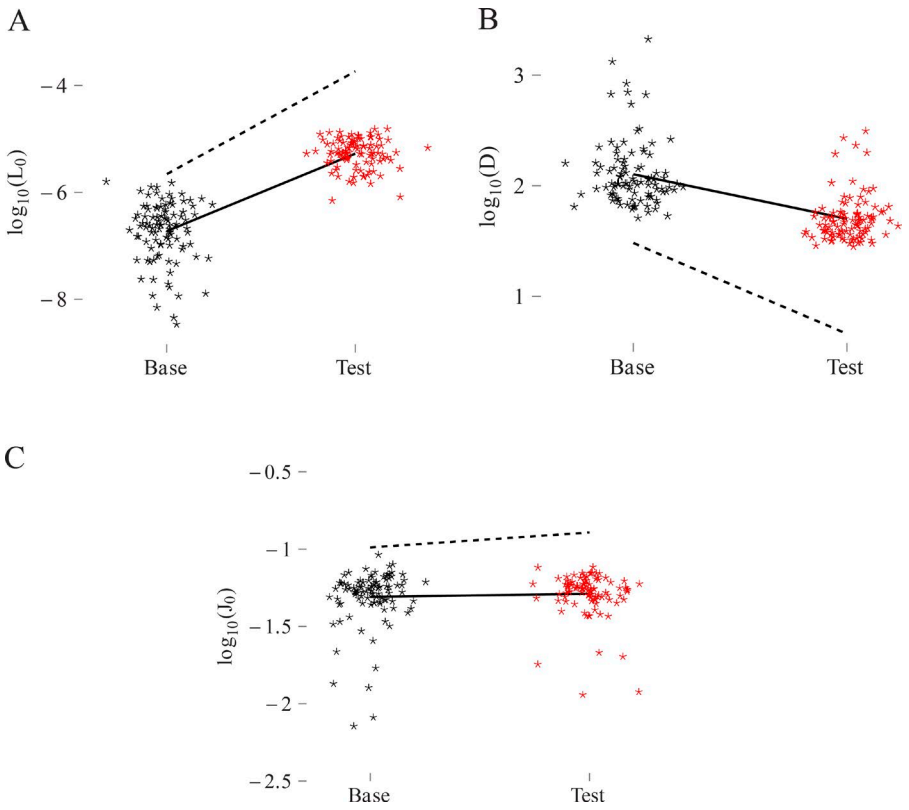

Figure 8. **Inferred parameters from the reduced log(P_o) model.** Values inferred by fitting the once-reduced log(P_o) model to 100 noisy synthetic measurements generated from base (black) and test (red) parameter sets. A–C correspond to inferred values of L_0, D, J_0, respectively. Solid lines connect the means of the inferred base and test values; dotted lines connect the true generating base and test values. The test parameter set used was, in: $L_0 = 10^{-3.7}$; $z_L = 10^{-0.1}$ e; $J_0 = 10^{-0.89}$; $z_J = 10^{-0.12}$ e; $K_D = 10^{-4.2}$ M; $C = 10^{0.79}$; $D = 10^{0.66}$; $E = 10^{0.54}$. The horizontal spread is only for ease of visualization.

may expect that a change in temperature or sequence that marginally effects the P_o data nonetheless largely increases C but equivalently decreases E.

To test for the presence of a compensatory effect, an experimentalist generally needs at least two assays: a "physiologically relevant" assay whose output should not change upon environmental manipulation, from which compensatory effects may be predicted, and one or more secondary assays, from which the differences in individual parameters can be observed. Obvious candidates for physiologically relevant assays include binding curves (as analyzed here) and physiologically and thermodynamically relevant functions thereof (Wyman, 1967; Di Cera, 1995; Chowdhury and Chanda, 2012). For BK, our results demonstrate that the log(P_o) assay serves as a good secondary assay for testing compensatory mechanisms predicted from the P_o assay.

Measurements of hemoglobin's oxygen-binding curve confirms that parameter compensations facilitate functional adaptation

How speculative is this prediction? On one hand, the existence of MBAM-identified parameter compensations is general. Compensations depend only on the underlying sloppiness of the model and assay, which have been demonstrated to be ubiquitous in multiparameter models across systems biology (Gutenkunst et al., 2007). On the other hand, the relevance of MWC parameter compensations in allosteric macromolecules is ultimately a question for experiment. To that end, we note that an extensive meta-analysis of hemoglobin's oxygen binding confirms the physiological relevance of MWC parameter compensations (Milo et al., 2007).

Milo et al. (2007) analyzed hemoglobin binding curves under varying physiological conditions and in different mammals. To quantitatively study these binding curves, Milo et al. (2007) used an MWC model that assumed the hemoglobin tetramer to be in one of two conformations: relaxed or tense. In each conformation, all four subunits have the same independent affinity for oxygen. The dissociation constants for the relaxed and tense states are K_R, K_T, respectively. The equilibrium constant between the fully deoxygenated tense and relaxed states is L_0. The three mechanistic parameters K_R, K_T, L_0 fully parameterize the model.

The authors found that this three-parameter model was non-identifiable with respect to the saturation curve. Using limit-style arguments that are possible for simple models and essentially equivalent to MBAM (Transtrum and Qiu, 2016), the model was reparameterized to have the emergent, identifiable parameters

$$L_4 = L_0 \cdot \frac{K_R^4}{K_T^4}, \quad L_{T0R4} = L_0 K_R^4. \tag{3}$$

The authors demonstrated analytically that each emergent parameter has a clear physiological interpretation: L_{T0R4} controls the half-saturation point of oxygen binding p_{50}; L_4 controls the cooperativity at this point, n.

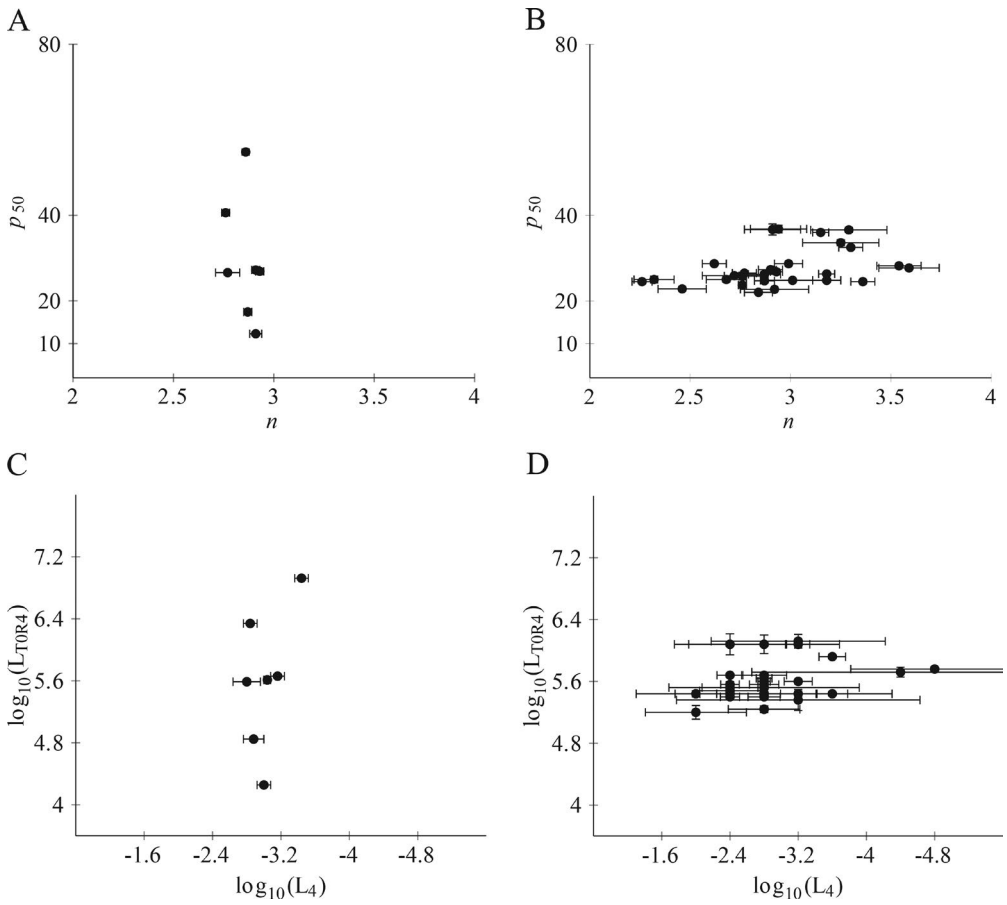

Figure 9. **Analysis of hemoglobin oxygen saturation curves.** These figures were generated with data published by Milo et al. (2007). (A and B) Reproduction of Milo et al. (2007) Fig. 2 (a and b). (C and D) Reproduction of Milo et al. (2007) Fig. 4 (a and b). (A and C) Each point corresponds to human hemoglobin at a different pH. (B and D) Each point corresponds to hemoglobin from a different mammal, at the same physiological condition. We refer the reader to the appropriate figures in Milo et al. (2007) for full descriptions of pH conditions and mammals used.

Moreover, the authors found that n remained constant for human hemoglobin at varying pH (Fig. 9 A).

The results of Milo et al. (2007) therefore present an exceptionally simple framework in which to test our prediction. The n assay remains constant upon physiological variation and is controlled by the single emergent parameter L_4. Is this assay constancy the result of compensations of the underlying MWC parameters, as we predict?

Indeed it is. Across varying pH conditions, n stays constant while p_{50} varies. Correspondingly, L_4 stays constant as L_{T0R4} varies (Fig. 9 C). It is immediate from the definitions of L_4 and L_{T0R4} (Eq. 3) that in order for L_4 to remain constant as L_{T0R4} varies, $K_T{}^4$ must compensate for changes in $L_0 \cdot K_R{}^4$.

Emergent parameters may identify evolutionary relevant "neutral spaces"

There is now significant theoretical (Draghi et al., 2010) and experimental (Hayden et al., 2011) evidence, including in allosteric proteins (Raman et al., 2016), that biological systems may evolve by drifting in genotype space such that their primary function remains unchanged. This is known as "neutral evolution" (Wagner, 2005, 2008). Neutral evolution proceeds via mutations that leave current function unchanged but may be advantageous in a subsequent environment. Because the utility of these mutations do not manifest until the correct environment arises, they are said to be cryptic. The spaces of sequences, parameters, or network topologies that give rise to equivalent behaviors are known as neutral spaces (Daniels et al., 2008).

Emergent parameters identified here may define neutral spaces. In particular, cryptic mutations in allosteric macromolecules may give rise to cryptic MWC parameter variations—large but compensatory effects in mechanistic parameters such that the value of MBAM-identified emergent parameters remain constant. This proposal can be tested by searching for cryptic MWC parameter changes between variants of an allosteric macromolecule within and across populations.

At first glance, the study of Milo et al. (2007) provides a way to interrogate this prediction as well. Milo et al. (2007) noted that the assay p_{50} stayed relatively

constant across 25 different mammals, measured at the same physiological conditions (Fig. 9 B). So too did the emergent parameter that controls it: L_{T0R4} (Fig. 9 D). This is indeed what we would expect if the emergent parameter identified a neutral space.

Unfortunately, the study by Milo et al. (2007) cannot be used to confirm the presence of a neutral space. If the L_{T0R4} constancy reflected a neutral space, we would expect L_0 and K_R^4 to vary cryptically between species. Because L_0 and K_R cannot be estimated from the available data, we cannot determine whether p_{50}'s constancy across species results from this cryptic variation or from L_0 and K_R^4 each remaining constant. The connection between emergent parameters and neutral spaces remains speculative, though we suspect it may prove an interesting source of future work.

Conclusions

We have argued that parameter compensation underlies both non-identifiability and adaptability in allosteric macromolecules. We therefore contend that non-identifiability should be expected in any adaptable allosteric macromolecule, so long as the model is mechanistically relevant and the functional assay adequately captures the macromolecule's function.

Non-identifiability does not itself imply that a model or assay is physiologically relevant. Experimentally verifying that a predicted parameter compensation is actually used, as we have done with hemoglobin and its cooperativity at the half saturation point of oxygen binding, n, is paramount. It must also be kept in mind that observed parameter compensations may be spurious rather than meaningful and must be assessed in context. In hemoglobin, the mechanistic relevance of the model parameters and clear physiological relevance of the half saturation point of oxygen binding support the relevance of the compensation we identified.

The enormous success of MWC models in describing allosteric macromolecules presents a wide array of opportunities for further experimentally testing the functional utility of parameter compensations. We anticipate that reduced models will prove essential for extracting mechanistically meaningful quantitative information from MWC models and provide a wealth of readily falsifiable predictions about the emergent properties of allosteric macromolecules.

ACKNOWLEDGMENTS

We would like to thank Miguel Holmgren and Paul Whittredge for discussions and careful reading of previous versions of the manuscript. We thank Daniel Silverman for helpful discussions and Susan Barnes for editorial assistance.

This work was supported by the Gatsby Charitable Foundation.

The authors declare no competing financial interests.

Author contributions: Both authors contributed equally to this work and contributed to all aspects of the work.

Richard W. Aldrich served as editor.

Submitted: 28 December 2016
Revised: 15 February 2017
Accepted: 8 March 2017

REFERENCES

Apgar, J.F., D.K. Witmer, F.M. White, and B. Tidor. 2010. Sloppy models, parameter uncertainty, and the role of experimental design. *Mol. Biosyst.* 6:1890–1900. http://dx.doi.org/10.1039/b918098b

Ball, F.G., and J.A. Rice. 1992. Stochastic models for ion channels: introduction and bibliography. *Math. Biosci.* 112:189–206. http://dx.doi.org/10.1016/0025-5564(92)90023-P

Ball, F.G., and M.S. Sansom. 1989. Ion-channel gating mechanisms: model identification and parameter estimation from single channel recordings. *Proc. R. Soc. Lond. B Biol. Sci.* 236:385–416. http://dx.doi.org/10.1098/rspb.1989.0029

Blatz, A.L., and K.L. Magleby. 1986. Correcting single channel data for missed events. *Biophys. J.* 49:967–980. http://dx.doi.org/10.1016/S0006-3495(86)83725-0

Brown, K.S., and J.P. Sethna. 2003. Statistical mechanical approaches to models with many poorly known parameters. *Phys. Rev. E Stat. Nonlin. Soft Matter Phys.* 68:021904. http://dx.doi.org/10.1103/PhysRevE.68.021904

Celentano, J.J., and A.G. Hawkes. 2004. Use of the covariance matrix in directly fitting kinetic parameters: application to GABAA receptors. *Biophys. J.* 87:276–294. http://dx.doi.org/10.1529/biophysj.103.036632

Changeux, J.-P. 2012. Allostery and the Monod-Wyman-Changeux model after 50 years. *Annu. Rev. Biophys.* 41:103–133. http://dx.doi.org/10.1146/annurev-biophys-050511-102222

Changeux, J.-P. 2013. 50 years of allosteric interactions: the twists and turns of the models. *Nat. Rev. Mol. Cell Biol.* 14:819–829. http://dx.doi.org/10.1038/nrm3695

Changeux, J.P., and S.J. Edelstein. 2005. Allosteric mechanisms of signal transduction. *Science.* 308:1424–1428. http://dx.doi.org/10.1126/science.1108595

Chowdhury, S., and B. Chanda. 2012. Estimating the voltage-dependent free energy change of ion channels using the median voltage for activation. *J. Gen. Physiol.* 139:3–17. http://dx.doi.org/10.1085/jgp.201110722

Colquhoun, D., and A.G. Hawkes. 1982. On the stochastic properties of bursts of single ion channel openings and of clusters of bursts. *Philos. Trans. R. Soc. Lond. B Biol. Sci.* 300:1–59. http://dx.doi.org/10.1098/rstb.1982.0156

Colquhoun, D., and A.G. Hawkes. 1995. The principles of the stochastic interpretation of ion-channel mechanism. *In* Single-Channel Recordings. B. Sakmann, and E. Neher, editors. Springer US, New York. 397–482. http://dx.doi.org/10.1007/978-1-4419-1229-9_18

Colquhoun, D., and F.J. Sigworth. 1995. Fitting and statistical analysis of single channel records. *In* Single-Channel Recording. B. Sakmann, and E. Neher, editors. Springer US, New York. 483–587. http://dx.doi.org/10.1007/978-1-4419-1229-9_19

Colquhoun, D., C.J. Hatton, and A.G. Hawkes. 2003. The quality of maximum likelihood estimates of ion channel rate constants. *J. Physiol.* 547:699–728. http://dx.doi.org/10.1113/jphysiol.2002.034165

Daniels, B.C., Y.-J. Chen, J.P. Sethna, R.N. Gutenkunst, and C.R. Myers. 2008. Sloppiness, robustness, and evolvability in systems biology. *Curr. Opin. Biotechnol.* 19:389–395. http://dx.doi.org/10.1016/j.copbio.2008.06.008

Di Cera, E. 1995. Thermodynamic Theory of Site-Specific Binding Processes in Biological Macromolecules. Cambridge University Press, Cambridge. 296 pp. http://dx.doi.org/10.1017/CBO9780511524837

Draghi, J.A., T.L. Parsons, G.P. Wagner, and J.B. Plotkin. 2010. Mutational robustness can facilitate adaptation. *Nature.* 463:353–355. http://dx.doi.org/10.1038/nature08694

Guo, H.H., J. Choe, and L.A. Loeb. 2004. Protein tolerance to random amino acid change. *Proc. Natl. Acad. Sci. USA.* 101:9205–9210. http://dx.doi.org/10.1073/pnas.0403255101

Gutenkunst, R.N., J.J. Waterfall, F.P. Casey, K.S. Brown, C.R. Myers, and J.P. Sethna. 2007. Universally sloppy parameter sensitivities in systems biology models. *PLOS Comput. Biol.* 3:e189. http://dx.doi.org/10.1371/journal.pcbi.0030189

Hayden, E.J., E. Ferrada, and A. Wagner. 2011. Cryptic genetic variation promotes rapid evolutionary adaptation in an RNA enzyme. *Nature.* 474:92–95. http://dx.doi.org/10.1038/nature10083

Hines, K.E., T.R. Middendorf, and R.W. Aldrich. 2014. Determination of parameter identifiability in nonlinear biophysical models: A Bayesian approach. *J. Gen. Physiol.* 143:401–416. http://dx.doi.org/10.1085/jgp.201311116

Horn, R., and K. Lange. 1983. Estimating kinetic constants from single channel data. *Biophys. J.* 43:207–223. http://dx.doi.org/10.1016/S0006-3495(83)84341-0

Horrigan, F.T., and R.W. Aldrich. 2002. Coupling between voltage sensor activation, Ca^{2+} binding and channel opening in large conductance (BK) potassium channels. *J. Gen. Physiol.* 120:267–305 (published erratum appears in *J. Gen. Physiol.* 2002. 120:599). http://dx.doi.org/10.1085/jgp.20028605

Kienker, P. 1989. Equivalence of aggregated Markov models of ion-channel gating. *Proc. R. Soc. Lond. B Biol. Sci.* 236:269–309. http://dx.doi.org/10.1098/rspb.1989.0024

Latorre, R., and S. Brauchi. 2006. Large conductance Ca^{2+}-activated K^+ (BK) channel: activation by Ca^{2+} and voltage. *Biol. Res.* 39:385–401. http://dx.doi.org/10.4067/S0716-97602006000300003

Machta, B.B., R. Chachra, M.K. Transtrum, and J.P. Sethna. 2013. Parameter space compression underlies emergent theories and predictive models. *Science.* 342:604–607. http://dx.doi.org/10.1126/science.1238723

Marquardt, D.W. 1963. An algorithm for least-squares estimation of nonlinear parameters. *J. Soc. Ind. Appl. Math.* 11:431–441. http://dx.doi.org/10.1137/0111030

Martins, B.M.C., and P.S. Swain. 2011. Trade-offs and constraints in allosteric sensing. *PLOS Comput. Biol.* 7:e1002261. http://dx.doi.org/10.1371/journal.pcbi.1002261

Marzen, S., H.G. Garcia, and R. Phillips. 2013. Statistical mechanics of Monod-Wyman-Changeux (MWC) models. *J. Mol. Biol.* 425:1433–1460. http://dx.doi.org/10.1016/j.jmb.2013.03.013

Middendorf, T.R., and R.W. Aldrich. 2017a. Structural identifiability of equilibrium ligand-binding parameters. *J. Gen. Physiol.* 149:105–119. http://dx.doi.org/10.1085/jgp.201611702

Middendorf, T.R., and R.W. Aldrich. 2017b. The structure of binding curves and practical identifiability of equilibrium ligand-binding parameters. *J. Gen. Physiol.* 149:121–147. http://dx.doi.org/10.1085/jgp.201611703

Milescu, L.S., G. Akk, and F. Sachs. 2005. Maximum likelihood estimation of ion channel kinetics from macroscopic currents. *Biophys. J.* 88:2494–2515. http://dx.doi.org/10.1529/biophysj.104.053256

Milo, R., J.H. Hou, M. Springer, M.P. Brenner, and M.W. Kirschner. 2007. The relationship between evolutionary and physiological variation in hemoglobin. *Proc. Natl. Acad. Sci. USA.* 104:16998–17003. http://dx.doi.org/10.1073/pnas.0707673104

Miranda, P., J.E. Contreras, A.J.R. Plested, F.J. Sigworth, M. Holmgren, and T. Giraldez. 2013. State-dependent FRET reports calcium- and voltage-dependent gating-ring motions in BK channels. *Proc. Natl. Acad. Sci. USA.* 110:5217–5222. http://dx.doi.org/10.1073/pnas.1219611110

Moffatt, L. 2007. Estimation of ion channel kinetics from fluctuations of macroscopic currents. *Biophys. J.* 93:74–91. http://dx.doi.org/10.1529/biophysj.106.101212

Monod, J., J.-P. Changeux, and F. Jacob. 1963. Allosteric proteins and cellular control systems. *J. Mol. Biol.* 6:306–329. http://dx.doi.org/10.1016/S0022-2836(63)80091-1

Monod, J., J. Wyman, and J.P. Changeux. 1965. On the nature of allosteric transitions: A plausible model. *J. Mol. Biol.* 12:88–118. http://dx.doi.org/10.1016/S0022-2836(65)80285-6

Olsman, N., and L. Goentoro. 2016. Allosteric proteins as logarithmic sensors. *Proc. Natl. Acad. Sci. USA.* 113:E4423–E4430. http://dx.doi.org/10.1073/pnas.1601791113

Qin, F., A. Auerbach, and F. Sachs. 1996. Estimating single-channel kinetic parameters from idealized patch-clamp data containing missed events. *Biophys. J.* 70:264–280. http://dx.doi.org/10.1016/S0006-3495(96)79568-1

Qin, F., A. Auerbach, and F. Sachs. 2000. A direct optimization approach to hidden Markov modeling for single channel kinetics. *Biophys. J.* 79:1915–1927. http://dx.doi.org/10.1016/S0006-3495(00)76441-1

Raman, A.S., K.I. White, and R. Ranganathan. 2016. Origins of allostery and evolvability in proteins: A case study. *Cell.* 166:468–480. http://dx.doi.org/10.1016/j.cell.2016.05.047

Rennell, D., S.E. Bouvier, L.W. Hardy, and A.R. Poteete. 1991. Systematic mutation of bacteriophage T4 lysozyme. *J. Mol. Biol.* 222:67–88. http://dx.doi.org/10.1016/0022-2836(91)90738-R

Somero, G.N. 1995. Proteins and temperature. *Annu. Rev. Physiol.* 57:43–68. http://dx.doi.org/10.1146/annurev.ph.57.030195.000355

Suckow, J., P. Markiewicz, L.G. Kleina, J. Miller, B. Kisters-Woike, and B. Müller-Hill. 1996. Genetic studies of the Lac repressor. XV: 4000 single amino acid substitutions and analysis of the resulting phenotypes on the basis of the protein structure. *J. Mol. Biol.* 261:509–523. http://dx.doi.org/10.1006/jmbi.1996.0479

Tkacik, G., C.G. Callan Jr., and W. Bialek. 2008. Information capacity of genetic regulatory elements. *Phys. Rev. E Stat. Nonlin. Soft Matter Phys.* 78:011910. http://dx.doi.org/10.1103/PhysRevE.78.011910

Transtrum, M.K. 2016. Manifold boundaries give "gray-box" approximations of complex models. *arXiv.* https://arxiv.org/abs/1605.08705 (Preprint posted May 27, 2016).

Transtrum, M.K., and P. Qiu. 2014. Model reduction by manifold boundaries. *Phys. Rev. Lett.* 113:098701. http://dx.doi.org/10.1103/PhysRevLett.113.098701

Transtrum, M.K., and P. Qiu. 2016. Bridging Mechanistic and Phenomenological Models of Complex Biological Systems. *PLOS Comput. Biol.* 12:e1004915. http://dx.doi.org/10.1371/journal.pcbi.1004915

Transtrum, M.K., B.B. Machta, and J.P. Sethna. 2010. Why are nonlinear fits to data so challenging? *Phys. Rev. Lett.* 104:060201. http://dx.doi.org/10.1103/PhysRevLett.104.060201

Transtrum, M.K., B.B. Machta, and J.P. Sethna. 2011. Geometry of nonlinear least squares with applications to sloppy models and optimization. *Phys. Rev. E Stat. Nonlin. Soft Matter Phys.* 83:036701. http://dx.doi.org/10.1103/PhysRevE.83.036701

Transtrum, M.K., B.B. Machta, K.S. Brown, B.C. Daniels, C.R. Myers, and J.P. Sethna. 2015. Perspective: Sloppiness and emergent theories in physics, biology, and beyond. *J. Chem. Phys.* 143:010901. http://dx.doi.org/10.1063/1.4923066

Wagner, A. 2005. Robustness, evolvability, and neutrality. *FEBS Lett.* 579:1772–1778. http://dx.doi.org/10.1016/j.febslet.2005.01.063

Wagner, A. 2008. Robustness and evolvability: a paradox resolved. *Proc. Biol. Sci.* 275:91–100. http://dx.doi.org/10.1098/rspb.2007.1137

Waterfall, J.J., F.P. Casey, R.N. Gutenkunst, K.S. Brown, C.R. Myers, P.W. Brouwer, V. Elser, and J.P. Sethna. 2006. Sloppy-model universality class and the Vandermonde matrix. *Phys. Rev. Lett.* 97:150601. http://dx.doi.org/10.1103/PhysRevLett.97.150601

Weber, J.K., and V.S. Pande. 2012. Protein folding is mechanistically robust. *Biophys. J.* 102:859–867. http://dx.doi.org/10.1016/j.bpj.2012.01.028

Wyman, J. 1967. Allosteric linkage. *J. Am. Chem. Soc.* 89:2202–2218. http://dx.doi.org/10.1021/ja00985a037

Yan, J., and R.W. Aldrich. 2010. LRRC26 auxiliary protein allows BK channel activation at resting voltage without calcium. *Nature.* 466:513–516. http://dx.doi.org/10.1038/nature09162